Rare Metal Materials and Engineering
Volume 53, Issue 12, December 2024
Available online at www.rmme.ac.cn

Science Press

Cite this article as: Liu Hang, Yang Chaoyun, Zhang Yao, et al. Simulation of Bubble Dynamics and Electrolyte Flow in Rare Earth Electrolysis Cell with Horizontal Electrode[J]. Rare Metal Materials and Engineering, 2024, 53(12): 3291-3298. DOI: 10.12442/j.issn.1002-185X.20240023.

ARTICLE

Simulation of Bubble Dynamics and Electrolyte Flow in Rare Earth Electrolysis Cell with Horizontal Electrode

Liu Hang[1,2], Yang Chaoyun[1], Zhang Yao[3], Luan Yikun[1,2], Li Dianzhong[1,2]

[1] Shenyang National Laboratory for Materials Science, Institute of Metal Research, Chinese Academy of Sciences, Shenyang 110016, China; [2] School of Materials Science and Engineering, University of Science and Technology of China, Shenyang 110016, China; [3] Baotou Skyrock Rare Earth New Material Co., Ltd, Baotou 014060, China

Abstract: A 2D transient mathematical model was established to separately describe the anode bubble dynamics and the bubble-induced electrolyte motion in the rare earth electrolysis cell with horizontal electrode. Results indicate that with the increase in the anode inclined angle, the maximum bubble thickness is increased gradually. Furthermore, compared with the conventional anode, the inclined and chamfered anodes are conductive to the bubble length reduction and the bubble velocity improvement. Meanwhile, the bubble-induced electrolyte motion in the electrolysis cell can improve the distribution and transport process of oxyfluorides, thereby enhancing the current efficiency. Finally, a novel feeding method based on the electrolyte flow is proposed.

Key words: rare earth electrolysis cell; horizontal electrode; anode inclined angle; bubble behavior; electrolyte motion

Nowadays, molten salt electrolysis is an effective method to prepare rare earth metal (REM)[1]. In the most frequently used vertical electrode cell (VEC)[2], rare earth oxide dissolves in the ReF_3-LiF molten salts and reacts with excess F^- ions to form oxyfluoride (ReOF). O^{2-} ions can also be generated when the ReOF further reacts with F^- ions in the molten salts. Then, the O^{2-} ions are transported to the vertical surface of anodes and react with the carbon molecules of anodes, forming carbon monoxide (CO) and carbon dioxide (CO_2) bubbles[3]. These bubbles slide along the vertical surface of anodes and rise quickly[4–5]. Currently, many problems of VEC, such as large energy consumption[6], low current efficiency[7], and unstable conditions of the electrolysis process[8], have been researched but still cannot be solved. One of the main obstacles is that the anode is placed fixedly in the graphite furnace[9]. Therefore, anode to cathode distance (ACD) usually becomes inconsistent during the electrolysis process. With the increase in ACD, the Joule heat in the electrolysis cell is increased and the cell temperature rises, which at last consumes more energy and leads to the decrease in the current efficiency[10–11].

Over the years, significant improvements and changes in the structure of electrolysis cells have been reported for the enhancement in performance and current efficiency[12–13]. A new type of electrolysis cell, namely horizontal electrode cell (HEC), has been proposed, presenting great potential to affect the efficiency of electrochemical reaction[14]. Its unique feature is that the cathode and anode are arranged in horizontal direction in HEC, as shown in Fig. 1. The anode is placed above the cathode. ACD in HEC can remain constant in the common operations of the electrolytic process, which is beneficial to the energy saving[15]. The bubble morphology and behavior on the anode are closely related to the confirmation of ACD[16]. Bubbles are formed on the lower horizontal surface of the anode in HEC, which are different from those formed on the vertical surface in VEC[17]. Hence, a detailed investigation of the bubble dynamics is necessary to provide important theoretical guidance for the selection of ACD and the design of HEC[18]. However, restricted by the high temperature[19], the heavily corrosive environment, and the opaque nature of molten salts[20], industrial measurements for detailed bubble dynamics in the rare earth electrolysis cell are

Received date: January 13, 2024
Foundation item: National Natural Science Foundation of China (52101165); Inner Mongolia Science and Technology Major Project (2020ZD0010); Key Research Program of the Chinese Academy of Sciences (ZDRW-CN-2021-3)
Corresponding author: Li Dianzhong, Ph. D., Professor, Shenyang National Laboratory for Materials Science, Institute of Metal Research, Chinese Academy of Sciences, Shenyang 110016, P. R. China, E-mail: dzli@imr.ac.cn

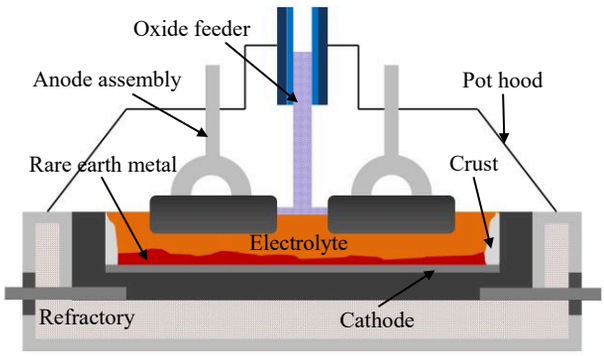

Fig.1 Rare earth electrolysis cell with horizontal electrode

expensive and can hardly be conducted[21]. Therefore, numerical model has been developed to predict the bubble behavior[22–24], benefiting from the significant improvement in computer hardware. Wang et al[25] conducted a 2D simulation to investigate the melt flow caused by bubbles. The related morphologies and velocity of bubbles were described for the comparison between innovative cell and traditional cell. The results indicated that the release of bubble was promoted by the novel design of aluminum electrolysis cell. Sun et al[26] investigated the bubble dynamics through the slotted anode. The bubble trajectory, bubble morphology, and bubble velocity were studied through a 3D transient mathematical model based on discrete phase model-discrete continuum transition model-volume of fluid (VOF) method. The results revealed that the slotted anode could decrease the bubble diameter. The longitudinal slot was much better for the bubble detachment than the transverse slot. However, most studies focus on the aluminum electrolysis cell[27]. The study on bubble morphology, behavior, and electrolyte flow of rare earth electrolysis cell is rarely reported.

In this research, a 2D transient gas-liquid two-phase flow mathematical model was established to investigate the bubble dynamics in HEC. The bubble-induced electrolyte motion was quantified. The simulation results provide theoretical foundation for the research and development of HEC, which is conducive to the science and technology innovation for the rare earth electrolysis industry.

1 Model Description

1.1 Fluid flow model

The bubble motion in the electrolysis cell involves a gas-liquid two-phase flow and two phases are not interpenetrating. Therefore, a 2D transient flow model was established to investigate the two-phase flow based on VOF method by solving the volume fraction continuity equation to capture the bubble shape. For each phase added to the model, a related variable is introduced to record the volume fraction of the phase in each control volume. The sum of volume fractions of all phases is 1 at each control volume. The fields for all variables and properties are shared by the phases and represent volume-averaged values, as long as the volume fraction of each phase is known at each location. Thus, the variables and properties in any given cell are representative of one specific phase or a mixture of phases, depending on the volume fraction values. Each phase agrees with the equation for mass conservation[28], as follows:

$$\frac{\partial \alpha}{\partial t} + \nabla\cdot(\alpha \boldsymbol{v}) = 0 \tag{1}$$

where α, t, and $\boldsymbol{v}$ are the phase volume fraction, time, and velocity, respectively. The primary phase volume fraction can be computed on the basis of specific constraint[29], as follows:

$$\alpha_g + \alpha_l = 1 \tag{2}$$

where α_g and α_l are volume fractions of gas and liquid phases, respectively. As all variables and properties are shared by the phases and represent volume-averaged values, the corresponding equation for conservation of momentum can be obtained[30], as follows:

$$\frac{\partial}{\partial t}(\rho \boldsymbol{v}) + \nabla\cdot(\rho \boldsymbol{v}\boldsymbol{v}) = -\nabla P + \nabla\cdot\left\{\mu\left[\nabla \boldsymbol{v} + (\nabla \boldsymbol{v})^{\mathrm{T}}\right]\right\} + \boldsymbol{F}_s + \rho \boldsymbol{g} \tag{3}$$

where P is the pressure; $\boldsymbol{F}_s$ represents the surface tension force; ρ and μ are the mixture density and viscosity, respectively. The mixture density and viscosity are based on the volume averaging[31], which can be expressed by Eq.(4–5), respectively:

$$\rho = \alpha_g \rho_g + \alpha_l \rho_l \tag{4}$$

$$\mu = \alpha_g \mu_g + \alpha_l \mu_l \tag{5}$$

where ρ_g and ρ_l are densities of gas and liquid phases, respectively; μ_g and μ_l are viscosities of gas and liquid phases, respectively. The simulation accuracy and efficiency strongly depend on the method of specific interpolation near the interfaces, which affects the convection and diffusion fluxes through the control volume fraction as well as the surface tension force $\boldsymbol{F}_s$ (included as a body force), as indicated in Eq.(1) and Eq.(3). The geometric reconstruction scheme and a mesh adaption method were adopted to capture the detailed interface shapes[32].

1.2 Boundary condition

In this research, the flow field was calculated by the commercial software FLUENT based on the finite volume method. The 2D simulation was used to investigate the motion of the bubble and electrolyte flow on account of computing efficiency and simulation accuracy[33]. Fig. 2 shows the simulation model of used HEC to study the bubble dynamics

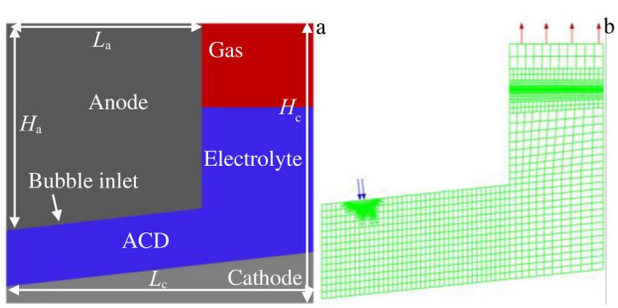

Fig.2 2D simulation model of HEC (a); adaptive mesh for simulation model (b)

and bubble-induced electrolyte motion. L_a and L_c are length of anode and cathode, respectively; H_a and H_c are height of anode and cathode, respectively. The geometrical and physical parameters of the simulation model are listed in Table 1[34–36]. The bottom surface of the anode was treated as no-slip wall for the electrolyte, namely the velocity inlet for the bubble. Moreover, the bubble was generated at one position of the bottom surface of anode. The equivalent diameter was defined as the diameter of a spherical bubble with an area equal to actual bubble area, because the observed bubbles were not spherical in the experiment[37]. The equivalent diameter of the bubble was assumed to be 5, 10, 15, and 20 mm, because the selected bubble diameters could truly reflect bubble layer beneath the anode during the industrial electrolysis process[38]. Anode inclined angle was assumed as 2°, 4°, 6°, 8°, and 10°, which are closer to the actual conditions[39].

The degassing momentum boundary condition was set for the outlet, which was considered as the wall for electrolyte and outlet for bubble. Other boundaries were assumed as no-slip wall for all fluids. During the simulation, the automatic mesh adaption method was used, allowing more accurate capture of the detailed interface between bubble and electrolyte and significantly reducing computing time. The global Courant number was set as 0.15 in this simulation. The flow was treated as laminar flow. The absolute convergence criteria for both continuity and velocity were set as 10^{-5}.

2 Results and Discussion

2.1 Bubble morphologies

Fig. 3 shows the predicted morphologies of bubble with diameter of 10 mm under the inclined anode of 2° in HEC. The whole motion process of the bubble is presented. After gas injection through the inlet, a small and more spherical bubble starts to grow, as shown in Fig. 3a. With the bubble growth, the bubble tends to flatten out. Once the bubble is sufficiently large, it begins to move along the bottom surface of the anode towards its higher end, as shown in Fig. 3b. Subsequently, the bubble is released at the anode edge (Fig. 3c) and keeps moving along the anode edge through the center channel (Fig. 3d). The formation of bubble is actually a complex dynamic balance process among surface tension, buoyancy force, viscous force between electrolyte and bubble,

Table 1 Geometrical and physical parameters of simulation model

Parameter	Value
Cell size, $L_c \times H_c$	300 mm×270 mm
Anode size, $L_a \times H_a$	200 mm×150 mm
ACD/mm	100
Electrolyte density/kg·m^{-3}	3850
Electrolyte viscosity/kg·(m·s)$^{-1}$	0.0049
Bubble density/kg·m^{-3}	0.4
Bubble viscosity/×10^{-5} kg·(m·s)$^{-1}$	1.37
Bubble-electrolyte surface tension/N·m^{-1}	0.4

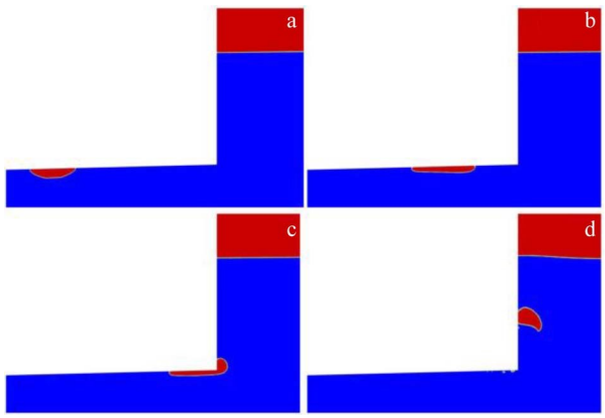

Fig.3 Predicted morphologies of bubble with 10 mm in diameter under anode with inclined angle of 2°: (a) t=1.0 s; (b) t=1.8 s; (c) t=2.3 s; (d) t=2.5 s

solid wall friction, and contact angle[40]. The combined effect of abovementioned parameters on bubble morphology is mainly determined by bubble diameter and anode inclined angle.

Fig. 4 shows bubble morphologies with bubble diameter of 5, 10, 15, and 20 mm under different anode inclined angles. Bubbles can maintain hemispherical shape when the diameter is 5 mm. With the increase in bubble diameter from 5 mm to 20 mm, bubble morphology gradually changes from ellipsoid to irregular spherical cap with thicker head and thinner tail[41]. This is because small bubbles have large specific surface, implying that unit volume of smaller bubbles receive greater surface tension. Thus, the small bubble is more easily to exhibit hemispherical shape than the big bubble[42]. Moreover, at the front end of the big bubble, the motion will be suppressed by the electrolyte, whereas the gas at the back side continuously moves forward. This phenomenon will cause the expansion of the big bubble head along the vertical direction. Thus, a thick head is formed[43]. Based on the simulation results, the bubble thickness is significantly uneven beneath the anode. The bubble profile relates to the bubble diameter and the anode inclined angle, which is consistent with the results in Ref.[26–28].

Fig. 5 illustrates the relationship between bubble length and inclined angle under different bubble diameters. It is evident that the increase in inclined angle decreases the bubble length under different bubble diameters. However, the length of small bubbles is less sensitive to the variation in anode inclined angle. The bubble lengths are maintained at approximately 19 and 36 mm when the bubble diameter is 5 and 10 mm, respectively. When the bubble diameter is 15 and 20 mm, the bubble length is decreased with the increase in anode inclined angle. For example, when the anode inclined angle increases from 2° to 10°, the bubble length with bubble diameter of 20 mm decreases from 78.81 mm to 65.91 mm (decrement=12.90 mm). This difference indicates that large inclined angle has a significantly positive effect on the reduction of covered area of anode by large bubbles.

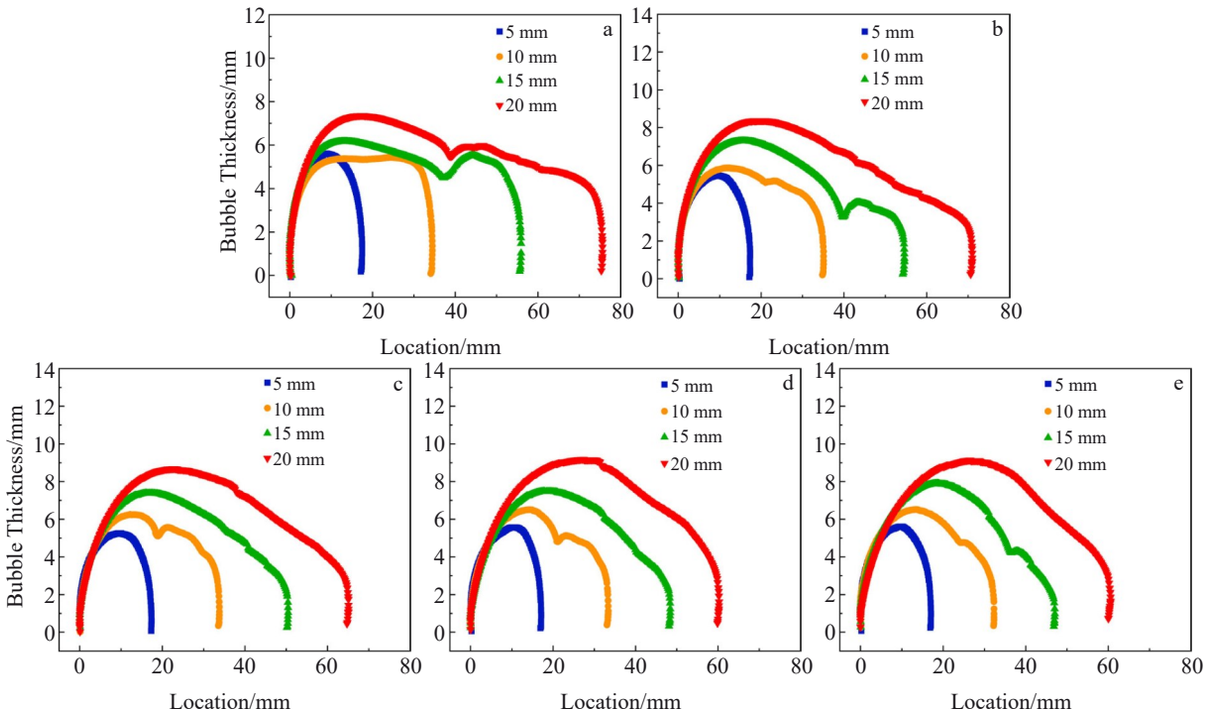

Fig.4 Bubble thickness curves with different bubble diameters under anode with inclined angle of 2° (a), 4° (b), 6° (c), 8° (d), and 10° (e)

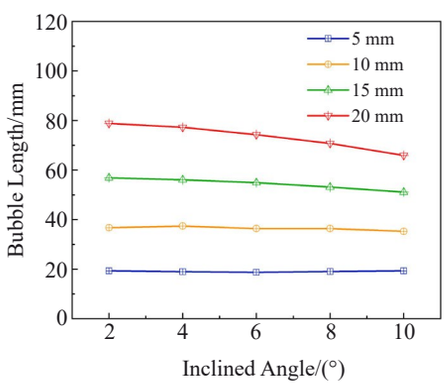

Fig.5 Effect of anode inclined angle on bubble length under different bubble diameters

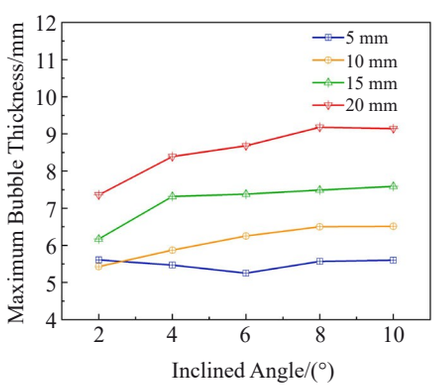

Fig.6 Effect of anode inclined angle on maximum bubble thickness under different bubble diameters

Fig. 6 illustrates the relationship between the maximum bubble thickness and inclined angle under different bubble diameters. The inclined anode structure barely has influence on the maximum bubble thickness for the bubble with 5 mm in diameter. The bubble presents a flat shape with the maximum bubble thickness of about 5.61 mm under different inclined angle conditions. As the bubble diameter exceeds 10 mm, the maximum bubble thickness is increased significantly with the increase in anode inclined angle. For example, when the anode inclined angle increases from 2° to 10° , the maximum bubble thickness with the bubble diameter of 20 mm increase from 7.36 mm to 9.14 mm. With the increase in inclined angle, the component of force perpendicular to the anode bottom is decreased and that parallel to the anode bottom is increased. The perpendicular component of the mass vector causes the variation in thickness. Thus, the greater the inclined angle, the larger the bubble thickness. The maximum bubble thickness ranges from 5.25 mm to 9.14 mm under all simulation conditions. Small bubbles coalesce to form big bubbles and then detach from the anode during industrial electrolysis process. The bubble may touch the bottom molten metal when ACD decreases to a certain threshold value, which consumes the molten metal through the secondary reaction. Because of the secondary reaction, the efficiency of the electrochemical reaction decreases, therefore affecting the current efficiency. To prevent the secondary reaction, ACD must be kept at a specific value in the usual operation of the electrolytic process, which is however detrimental to the energy saving. Hence, the maximum bubble thickness of large bubble plays an important role in the selection of ACD.

2.2 Bubble behavior

Fig.7 illustrates the relationship between the average bubble velocity and inclined angle under different bubble diameters. Under different bubble diameters, the bubble velocity has an obviously linear relationship with the inclined angle. The slope is increased with the increase in bubble diameter. Compared with small inclined angle, larger inclined angle leads to bigger difference in the bubble velocity. This phenomenon indicates that the increase in the bubble diameter has a more significant effect on the bubble removal under large inclined angle conditions. Bubbles in electrolyte are essentially air pockets with low density[44]. Therefore, the larger bubble contains more air and should rise more quickly, compared with the smaller bubbles. Furthermore, the large inclined angle can increase the resultant force acting on the bubble, thereby accelerating the bubble motion to the anode edge. Due to the poor electrical conductivity, the bubbles induce extra voltage drop, therefore leading to a significant amount of extra energy loss. Hence, it is essential to remove the bubble beneath the anodes in time.

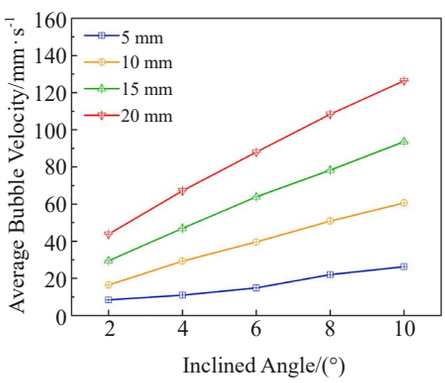

Fig.7 Effect of anode inclined angle on average bubble velocity under different bubble diameters

Fig. 8 compares the bubble velocity at the anode edge between conventional anode and chamfered anode under bubble diameter of 5, 10, 15, and 20 mm. The chamfered anode increases the bubble velocity under all bubble diameter conditions, compared with the conventional anode. The bubble movement direction gradually changes from horizontal direction to vertical direction when the bubble touches the edge of chamfered anode. Moreover, the chamfered anode can shorten the bubble motion distance. The chamfered anode mainly exerts reduction effect on the bubble residence time on the anode bottom, which promotes electrolyte access to the electrochemically active surface area, thereby significantly decreasing the required energy of the electrolysis process.

2.3 Electrolyte flow under bubble condition

Fig.9 shows the velocity fields of electrolyte with different bubble diameters under anode with various inclined angles in HEC. It is obvious that the velocity magnitude of the bubble is much larger than that of the surrounding electrolyte. Hence, the bubble head pushes the front electrolyte away, and the electrolyte flows backward under the bubble to fill the original position of bubbles. Considering the effect of viscosity, the electrolyte becomes more active. As a result, the shear force between the electrolyte and bubble becomes greater, thereby promoting the bubble motion. Moreover, local vortex also

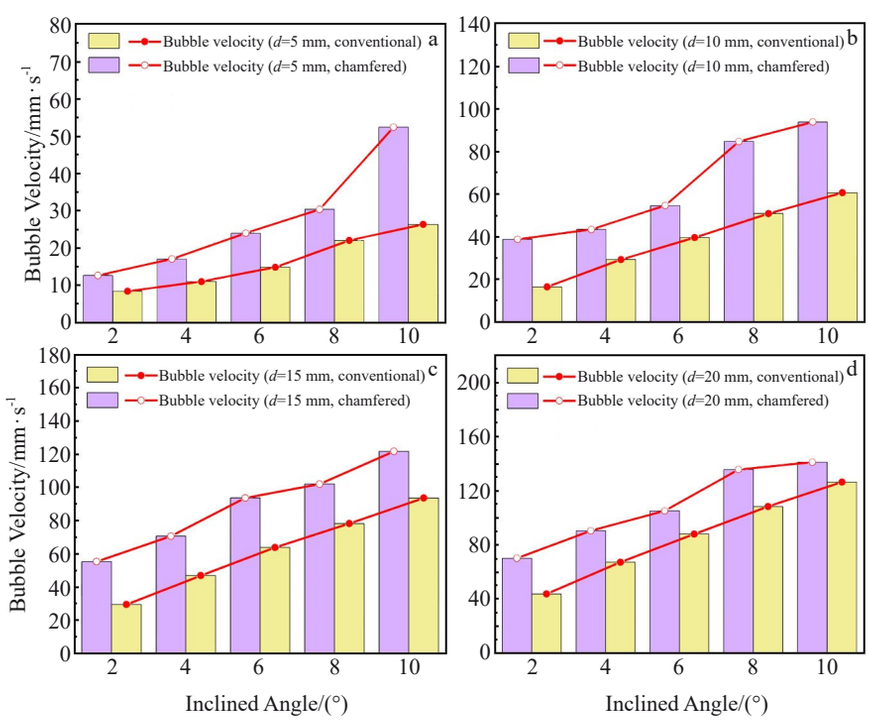

Fig.8 Comparison of bubble velocity with bubble diameter of 5 mm (a), 10 mm (b), 15 mm (c), and 20 mm (d) under conventional and chamfered anode

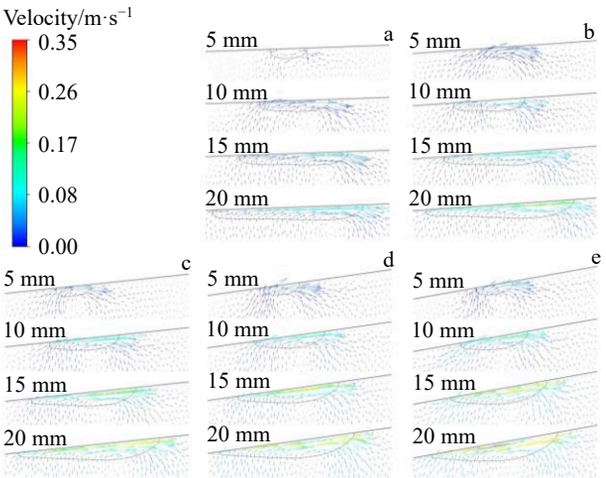

Fig.9 Velocity fields of electrolyte with different bubble diameters under anode with inclined angle of 2° (a), 4° (b), 6° (c), 8° (d), and 10° (e)

contributes to the transportation of electrolytic substance ReOF from the feeding region at the top of electrolysis cell to the electrolytic reaction region between anode and cathode.

Fig. 10 illustrates the relationship between maximum electrolyte velocity and inclined angle under different bubble diameters. The motion of electrolyte around the bubble is enhanced and becomes more active due to the bubble motion. The maximum velocity is significantly increased with the increase in anode inclined angle, as shown in Fig. 10a. The maximum electrolyte velocity around large bubble is larger than that around small bubble, which can be attributed to the large buoyancy force and velocity of large bubbles. Besides, the electrolyte flow field at the bottom of electrolysis cell also increases to some extent. The electrolyte moves faster because of the bubble, and then the bottom liquid metal is accelerated by the electrolyte through the interphase force. However, it is clear that the velocity of electrolyte near the bottom of electrolysis cell is smaller than that surrounding the bubble, as shown in Fig. 10b. Therefore, the interface fluctuation of bottom liquid metal can be reduced effectively, which is in favor of current efficiency improvement.

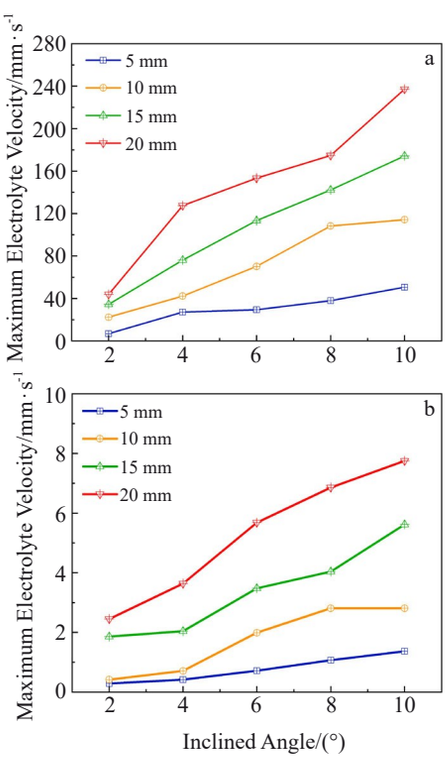

Fig.10 Relationship between maximum electrolyte velocity and inclined angle under different bubble diameters: (a) near the bubble and (b) near the bottom of electrolysis cell

Fig. 11 shows the velocity fields of the electrolyte surrounding bubbles during the bubble motion process under the conditions of anode inclined angle of 2° and bubble diameter of 10 mm. Fig. 12 shows the schematic diagrams of bubble, electrolyte, and ReOF trajectory in HEC. Bubble motion significantly affects the electrolyte flow field and the upper electrolyte will become more active. However, there is no bubble flow at the edge of electrolysis cell due to the inclined anode. The electrolyte velocity maintains a valley value at the position between the anode and the cell wall. Thus, a stagnant zone appears near the cell wall. Since the solubility of ReOF in molten fluorides is as low as 2wt%–4wt%[45], electrolyte crust can be formed on the side of electrolysis cell by feeding oxide from the side of cell at the

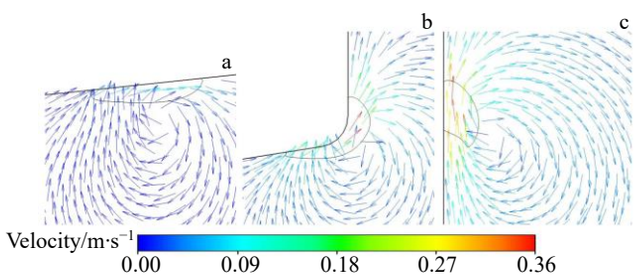

Fig.11 Velocity fields of electrolyte during bubble motion process with bubble diameter of 10 mm under inclined angle of 2°: (a) beneath anode; (b) at the anode edge; (c) in the center channel

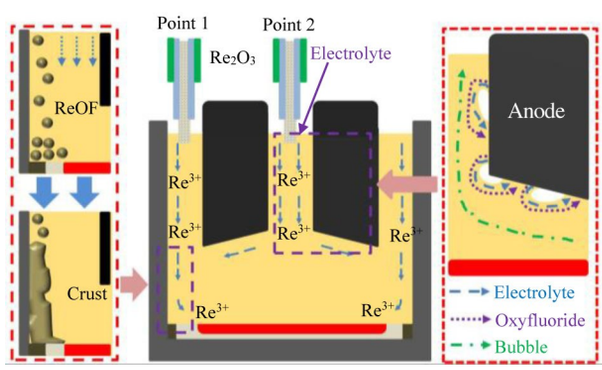

Fig.12 Schematic diagrams of bubble, electrolyte, and ReOF trajectory during electrolysis process

early stage of electrolysis. The formation of crust on the electrolysis cell wall surface is conducive to the reduction of horizontal current, and the current efficiency of electrolysis process is also improved.

The electrolyte located in the upper part between the anode and cathode moves upward along the slope of anode to the top side under the action of bubble. According to the direction of electrolyte flow, two flow modes of electrolyte can be distinguished. Partial electrolyte reaches the top of electrolysis cell through the gap between anodes and then returns to the zone between anode and cathode. Other electrolyte enters the region between anodes and flows back to the region between anode and cathode directly. These electrolytes merge and then flow to the bottom surface of anode. Therefore, the bubble motion leads to the circulating movement in molten electrolyte, which can accelerate the dissolution and diffusion of ReOF, thereby contributing to the transport process of O^{2-} ions to the bottom surface of anodes where the chemical reaction occurs. The motion process of electrolyte provides guidance for REM preparation in HEC. Besides, according to the simulation results, it is beneficial to feed oxides at the center of electrolysis cell to achieve the uniform distribution of ReOF.

3 Conclusions

1) The increase in anode inclined angle can decrease bubble length and increase bubble thickness in HEC, particularly when the bubble diameter is 10 – 20 mm. The maximum bubble thickness ranges from 5.25 mm to 9.14 mm under all simulation conditions.

2) Bubble velocity is promoted by the anode inclined anode: the larger the anode inclined angle, the faster the bubble velocity. Moreover, the chamfered anode can further increase bubble velocity at the anode edge.

3) The electrolyte motion is promoted by bubble motion in HEC. Bubble motion can cause a local vortex in molten electrolyte, thereby accelerating the transportation of ReOF from the feeding region at the top of electrolysis cell to the reaction region located between anode and cathode.

4) A novel feeding method based on the electrolyte motion is developed, which includes feeding oxide on the side of electrolysis cell at the early electrolysis stage to form crust and then feeding oxide at the center of electrolysis cell to achieve the uniform distribution of ReOF.

References

1 Liu H, Zhang Y, Luan Y K *et al*. *Metals*[J], 2020, 10(10): 1376

2 Zuo Z P, Liu Y B, Yang X *et al*. *Journal of Rare Earths*[J], 2022, 40(6): 996

3 Liu S Z, Chen L Y, Li B *et al*. *Electrochimica Acta*[J], 2014, 147: 82

4 Zhou J, Meng X H, Zhang R *et al*. *Electrocatalysis*[J], 2021, 12(6): 628

5 Ding L, Wang X P, Yan Y D *et al*. *Journal of Rare Earths*[J], 2023, 41(8): 1250

6 Li M, Liu C Y, Ding A T *et al*. *Journal of Environmental Chemical Engineering*[J], 2023, 11(3): 109746

7 Abbasalizadeh A, Seetharaman S, Venkatesan P *et al*. *Electrochimica Acta*[J], 2019, 310: 146

8 Han W, Li M, Zhang M L *et al*. *Rare Metals*[J], 2016, 35(11): 811

9 Sahoo D K, Singh H, Krishnamurthy N. *Rare Metals*[J], 2013, 32(3): 305

10 Sarfo P, Das A, Young C. *Separation and Purification Technology*[J], 2021, 256: 117770

11 Liu Y L, Ren H, Yin T Q *et al*. *Electrochimica Acta*[J], 2019, 326: 134971

12 Liu Zhongxing, Qi Suci. *Rare Metal Materials and Engineering*[J], 2007, 36(2): 194 (in Chinese)

13 Li Zejin, Dan Linyang, Li Xuemin *et al*. *Rare Metal Materials and Engineering*[J], 2017, 46(12): 3767 (in Chinese)

14 Kang Jia, Liu Yubao, Yu Bing *et al*. *Materials China*[J], 2022, 41(2): 148 (in Chinese)

15 Xu H B, Zhang W, Wang C S *et al*. *Appl Radiat Isot*[J], 2022, 182: 110149

16 Sun M J, Li B K, Liu Z Q. *Powder Technology*[J], 2023, 428: 118854

17 Zhao Z B, Wang Z W, Gao B L *et al*. *Metallurgical and Materials Transactions B*[J], 2016, 47(3): 1962

18 Tao W J, Li T F, Wang Z L *et al*. *Metallurgical and Materials Transactions B*[J], 2015, 47(1): 23

19 Liu X, Xue J L, Guo Z C *et al*. *Journal of Materials Science & Technology*[J], 2019, 35(7): 1422

20 Yang S H, Yang F L, Liao C F *et al*. *Journal of Rare Earths*[J], 2010, 28(S1): 385

21 Yasuda K, Oishi T, Kagotani T *et al*. *Journal of Alloys and Compounds*[J], 2021, 889: 161605

22 Bo Y X, Wu X, Zhou Y H *et al*. *Flow Measurement and Instrumentation*[J], 2022, 85: 102156

23 Garoosi F, Merabtene T, Mahdi T F. *Ocean Engineering*[J], 2022, 247: 110711

24 Li X N, Liu M Y, Dong T T *et al*. *Chemical Engineering Research and Design*[J], 2020, 155: 108

25 Wang Q, Li B K, He Z *et al*. *Metallurgical and Materials Transactions B*[J], 2013, 45(1): 272

26 Sun M J, Li B K, Liu Z Q *et al*. *Chemical Engineering Journal*[J], 2022, 428: 131182

27 Wang Q, Sun M J, Li B K *et al*. *Transactions of Nonferrous Metals Society of China*[J], 2018, 28(8): 1670

28 Mulbah C, Kang C, Mao N *et al*. *Progress in Nuclear Energy*[J], 2022, 154: 104478

29 Vaishnavi G N V S, Ramarajan J, Jayavel S. *Thermal Science and Engineering Progress*[J], 2023, 39: 101718

30 Brackbill J U, Kothe D B, Zemach C. *Journal of Computational Physics*[J], 1992, 100(2): 335

31 Hirt C W, Nichols B D. *Journal of Computational Physics*[J], 1981, 39(1): 201
32 Rajamani K, Jasper M. *Nature*[J], 1999, 398(6724): 208
33 Le Thanh K C, Parzani C, Vignal M H. *Journal of Computational Physics*[J], 2007, 225(2): 1937
34 Huttenhuis P J G, Kuipers J A M, Swaaij W P M. *Chemical Engineering Science*[J], 1996, 51(24): 5273
35 Zhu X P, Sun S C, Sun T *et al*. *Journal of Rare Earths*[J], 2020, 38(6): 676
36 Zhu X, Sun S, Lu S *et al*. *Thermochimica Acta*[J], 2016, 636: 42
37 Subramaniam A B, Abkarian M, Mahadevan L *et al*. *Nature*[J], 2005, 438(7070): 930
38 Zhang K, Feng Y, Schwarz P *et al*. *Industrial & Engineering Chemistry Research*[J], 2013, 52(33): 11378
39 Sun M J, Li B K, Li L *et al*. *Metallurgical and Materials Transactions B*[J], 2017, 48(6): 3161
40 Gaurav K, Mittal G, Karn A. *Chemical Engineering Science*[J], 2022, 250: 117395
41 Vékony K, Kiss L I. *Metallurgical and Materials Transactions B*[J], 2010, 41(5): 1006
42 Orvalho S, Stanovsky P, Ruzicka M C. *Chemical Engineering Journal*[J], 2021, 406: 125926
43 Huang Y P, Wang Z W, Yang Y J *et al*. *Metals*[J], 2018, 8(10): 806
44 Osarinmwian C. *Applied Physics A*[J], 2017, 123: 150
45 Zhu X P, Sun S C, Liu C *et al*. *Journal of Rare Earths*[J], 2018, 36(7): 765

水平电极稀土电解槽阳极气泡动力学及电解液流动数值模拟

刘　航[1,2]，杨超云[1]，张　耀[3]，栾义坤[1,2]，李殿中[1,2]
(1. 中国科学院 金属研究所 沈阳材料科学国家研究中心，辽宁 沈阳 110016)
(2. 中国科学技术大学 材料科学与工程学院，辽宁 沈阳 110016)
(3. 包头天石稀土新材料有限责任公司，内蒙古 包头 014060)

摘　要：建立了一个二维瞬态数学模型，分别描述了水平电极稀土电解槽中阳极气泡动力学和气泡诱导的电解液运动。结果表明，随着阳极倾斜角度的增大，阳极气泡厚度逐渐增大。此外，与常规阳极相比，倾斜和倒角阳极有利于缩短气泡长度，提高气泡速度。同时，电解槽内气泡诱导的电解质运动可以改善稀土氟氧化物的分布和运动过程，从而提高电流效率。最后，基于电解液流动提出了一种新型的加料方式。

关键词：稀土电解槽；水平电极；阳极倾斜角度；气泡行为；电解质运动

作者简介：刘　航，男，1990年生，博士，中国科学院金属研究所沈阳材料科学国家研究中心，辽宁 沈阳 110016，电话：024-23971973，E-mail：liuhang@imr.ac.cn